EARTHQUAKE ENGINEERING AND STRUCTURAL DYNAMICS, VOL. 26, 917–929 (1997)

IMPROVED NUMERICAL DISSIPATION FOR EXPLICIT METHODS IN PSEUDODYNAMIC TESTS

SHUENN-YIH CHANG*†

National Center for Research on Earthquake Engineering, National Taiwan University, Taipei, Taiwan, ROC

SUMMARY

There is no second-order accurate, dissipative, explicit method in the currently available step-by-step integration algorithms. Two new families of second-order accurate, dissipative, explicit methods have been successfully developed for the direct integration of equations of motion in structural dynamics. These two families of methods are numerically equivalent and possess the desired numerical dissipation which can be continuously controlled. These two families of algorithms are very useful for pseudodynamic tests since the favourable numerical damping can be used to suppress the spurious growth of high-frequency modes due to the presence of numerical and/or experimental errors in performing a pseudodynamic test. © 1997 by John Wiley & Sons, Ltd.

Earthquake Engng. Struct. Dyn., **26**, 917–929 (1997)

No. of Figures: 7. No. of Tables: 0. No. of References: 15.

KEY WORDS: numerical dissipation; explicit method; pseudodynamic test

INTRODUCTION

Unlike in analytical methods, in pseudodynamic tests the restoring forces developed by the structure are measured experimentally after the displacements are computed and physically imposed on a test specimen. It is believed that pseudodynamic test methods can provide more accurate results than the analytical methods can. This is because of using measured restoring forces instead of the mathematical description of the non-linear model which is very hard to predict accurately. The major difficulty in solving a non-linear system, either using an analytical method or a pseudodynamic test method, is the error introduced by the assumption that the structural properties remain constant during each time step. These errors, which will be termed 'linearization errors', are carried over to subsequent computations and tend to accumulate from the initiation of errors to the end. Numerical results may diverge significantly from the correct solutions due to this cumulative effect and the large number of steps. For a highly non-linear system, this linearization problem is often overcome by using a very small time step or by using an iterative technique where the structural properties are updated in the time step to reduce or eliminate the linearization errors.

In general, the stiffness matrix of a non-linear system is very difficult to accurately determine in a pseudodynamic test. Furthermore, it is necessary to use an iterative technique for an implicit method to

* Correspondence to: Shuenn-Yih Chang, National Center for Research on Earthquake Engineering, National Taiwan University, 1, Roosevelt Road, Section 4, Taipei, Taiwan, R.O.C.
† Associate Research Fellow

Contract grant sponsor: National Science Council, Taiwan, R.O.C.; Contract grant number: NSC-86-2211-E-319-001

CCC 0098–8847/97/090917–13$17·50

Received 16 January 1996
Revised 7 November 1996

solve the equations of motion since the structural properties might be changed in each time step. The iterative technique can be used in an analytical analysis but it may lead to incorrect response history in the pseudodynamic testing since the behaviour of the specimen is highly path dependent for a non-linear system. These two difficulties exclude the use of implicit algorithms in the original development of pseudodynamic test method. Even though some implicit schemes have been developed recently,[1–4] their implementations are more complicated than that of explicit methods. Thus, explicit methods are widely used for pseudodynamic testing.

The high-frequency modes of spatially discretized equations generally do not represent the real behaviour of the original problem. In addition, the presence of numerical errors will lead to the spurious growth of high-frequency response and the inevitable experimental errors will aggravate this effect in pseudodynamic tests. Therefore, it is advantageous for an algorithm to possess numerical damping to suppress any spurious participation of the high-frequency response while the lower modes can be integrated accurately. Although it is natural to consider the use of viscous damping to remove the higher modes, Shing and Mahin[5] have shown that using a viscous damping matrix based on initial elastic structural properties for a non-linear system might lead to unreliable results as the structural properties change.

Many direct integration algorithms possess inherent numerical dissipation. The amount of numerical dissipation varies with algorithms and depends very much on the frequencies of a structural system. Several implicit algorithms exhibit this damping effect, such as the Wilson θ method,[6] Houbolt's method,[7] and the α-dissipation method.[8,9] Almost none of the explicit algorithms have the desired numerical damping. For example, the most commonly used central difference method does not possess any numerical dissipation. Although numerical dissipation can be introduced into the explicit form of the general Newmark's method with $\gamma > \frac{1}{2}$, the response of the lower modes is damped too strongly. For this reason, a modified Newmark explicit method[10,5] has been proposed for pseudodynamic testing. This algorithm can have arbitrary small numerical damping for the fundamental mode and significant numerical damping for the higher modes. However, the lower modes except the fundamental mode might be overdamped and might also show a significant period distortion error, since the numerical damping is almost linearly proportional to the natural frequency for a given time step. Furthermore, a negative damping effect might occur in a non-linear oscillation.[10,5] Therefore, its applications are inconvenient and limited.

The explicit algorithms proposed herein can have the desired numerical dissipation which can be continuously controlled by parameters other than the time step. In addition, they are second-order methods. The formulations of the new algorithms are the same as that of the α-dissipation method except that the parameters α, β, and γ are no longer constants. They are functions of the inverse of the mass and stiffness matrices of the structural system and the size of the integration time step.

ANALYSIS

The equations of motion for a linear multiple-degree-of-freedom (MDOF) system can be expressed in a matrix form as:

$$\mathbf{M}\ddot{\mathbf{u}} + \mathbf{C}\dot{\mathbf{u}} + \mathbf{K}\mathbf{u} = \mathbf{f} \tag{1}$$

where $\mathbf{M}$, $\mathbf{C}$, and $\mathbf{K}$ are the mass, viscous damping and stiffness matrices, $\mathbf{u}$, $\dot{\mathbf{u}}$ and $\ddot{\mathbf{u}}$ are the vectors of displacement, velocity and acceleration, respectively, and $\mathbf{f}$ is the external force excitation vector. The initial value problem for equation (1) is to find a solution $\mathbf{u} = \mathbf{u}(t)$ having the given initial conditions.

In the following analysis, an undamped linear Single-Degree-Of-Freedom (SDOF) system is considered. However, the results obtained are applicable to linear MDOF systems, in general, by means of mode superposition method.[11] The α-dissipation method can be used to solve the above initial value problem and

has the following formulations:

$$\begin{aligned} ma_{i+1} + (1+\alpha)kd_{i+1} - \alpha kd_i &= f_{i+1} \\ d_{i+1} = d_i + (\Delta t)v_i + (\Delta t)^2[(\tfrac{1}{2}-\beta)a_i + \beta a_{i+1}] \\ v_{i+1} = v_i + (\Delta t)[(1-\gamma)a_i + \gamma a_{i+1}] \end{aligned} \tag{2}$$

where m is the mass, k is the stiffness, f_i is the external excitation, and d_i, v_i, and a_i are the approximate solutions of displacement, velocity and acceleration, respectively. The subscript i indicates the time step at $t = i(\Delta t)$. The characteristics of numerical dissipation and stability of the algorithm are controlled by the parameters α, β and γ. If $\alpha = 0$ this family of algorithms reduces to the Newmark family.[12] In this case with $\beta = 0$, the algorithm is energy conserving if $\gamma = \frac{1}{2}$, whereas numerical dissipation is present if $\gamma > \frac{1}{2}$ and is the so called Newmark explicit method with γ-dissipation.

In the case of a free-vibration response, the step-by-step integration algorithm can be written in a recursive matrix form

$$\mathbf{X}_{i+1} = \mathbf{A}\mathbf{X}_i = \mathbf{A}^{i+1}\mathbf{X}_0 \tag{3}$$

where $\mathbf{X}_i = [d_i, (\Delta t)v_i, (\Delta t)^2 a_i]^{\mathrm{T}}$, $\mathbf{X}_0$ is the initial vector, and $\mathbf{A}$ is the amplification matrix. The explicit form of $\mathbf{A}$ is

$$\mathbf{A} = \left(\frac{1}{D}\right)\begin{bmatrix} 1+\alpha\beta\Omega^2 & 1 & \frac{1}{2}-\beta \\ -\gamma\Omega^2 & 1-(1+\alpha)(\gamma-\beta)\Omega^2 & (1-\gamma)-(1+\alpha)(\frac{1}{2}\gamma-\beta)\Omega^2 \\ -\Omega^2 & -(1+\alpha)\Omega^2 & -(1+\alpha)(\frac{1}{2}-\beta)\Omega^2 \end{bmatrix} \tag{4}$$

where $D = 1 + (1+\alpha)\beta\Omega^2$, $\Omega = \omega(\Delta t)$ and $\omega = \sqrt{k/m}$. The characteristic equation for the matrix $\mathbf{A}$ is

$$\det(\mathbf{A} - \lambda\mathbf{I}) = \lambda^3 - A_1\lambda^2 + A_2\lambda - A_3 = 0 \tag{5}$$

where λ denotes an eigenvalue of $\mathbf{A}$, $\mathbf{I}$ is an identity matrix, and A_1, A_2 and A_3 are as follows:

$$\begin{aligned} A_1 &= \frac{1}{D}\{2 + [(3\alpha+2)\beta - (1+\alpha)(\gamma+\tfrac{1}{2})\Omega^2]\} \\ A_2 &= \frac{1}{D}\{1 + [\alpha(3\beta-2\gamma) + (\beta-\gamma+\tfrac{1}{2})]\Omega^2\} \\ A_3 &= \frac{1}{D}[\alpha(\beta-\gamma+\tfrac{1}{2})\Omega^2] \end{aligned} \tag{6}$$

The approach to analyse stability and accuracy through the amplification matrix and the derivation of local truncation error can be found in References 13 and 8. The local truncation error for the α-dissipation method is found to be

$$E = \frac{\omega\Omega\dot{u}}{D}(\alpha+\gamma-\tfrac{1}{2}) + \frac{\omega^2\Omega^2 u}{D}[\tfrac{1}{2}(\alpha+\gamma-\tfrac{1}{2}) - \alpha(\gamma-\tfrac{1}{2}) - \beta + \tfrac{1}{12}] \tag{7}$$

The difference equation is consistent with the differential equation if $E = O[(\Delta t)^x]$ in which $x > 0$; x is called the order of accuracy or rate of convergence. Obviously, consistency implies that $E \to 0$ as $\Delta t \to 0$, and the order of accuracy is the rate at which the local truncation error goes to zero as $\Delta t \to 0$.

THE DEVELOPMENT OF EXPLICIT ALGORITHMS

Two new families of second-order, dissipative, explicit methods can be derived by the following procedure. It is necessary to assume $\beta = 0$ in the development of these methods since they are supposed to be explicit. In addition, second-order accuracy can be achieved if $\alpha + \gamma - \frac{1}{2}$ in equation (7) is chosen to be a polynomial function of Ω^m with zero constant where the superscript m must be greater or equal to 1. Due to the similarity in developing the new integration algorithms, only the detailed derivations of α-function dissipative method will be presented herein. However, the results for the γ-function dissipative method are provided.

α-function dissipative method

For the case of $\beta = 0$ and $\gamma = \frac{1}{2}$, equations (4) and (6) become

$$\mathbf{A} = \begin{bmatrix} 1 & 1 & \frac{1}{2} \\ -\frac{1}{2}\Omega^2 & 1 - \frac{1}{2}(1+\alpha)\Omega^2 & \frac{1}{2} - \frac{1}{4}(1+\alpha)\Omega^2 \\ -\Omega^2 & -(1+\alpha)\Omega^2 & -\frac{1}{2}(1+\alpha)\Omega^2 \end{bmatrix} \tag{8}$$

and

$$A_1 = 2 - (1+\alpha)\Omega^2, \qquad A_2 = 1 - \alpha\Omega^2, \qquad A_3 = 0 \tag{9}$$

and equation (5) reduces to

$$\lambda(\lambda^2 - A_1\lambda + A_2) = 0 \tag{10}$$

The algorithms of this family are explicit since β is zero. The eigenvalues of the matrix $\mathbf{A}$ are

$$\lambda_{1,2} = \left[1 - \left(\frac{1+\alpha}{2}\right)\Omega^2\right] \pm \mathrm{j}\Omega\sqrt{1 - \tfrac{1}{4}(1+\alpha)^2\Omega^2}, \qquad \lambda_3 = 0 \tag{11}$$

The first equation of equation (11) can be rewritten as

$$\lambda_{1,2} = \mathrm{a} \pm \mathrm{j}b = \mathrm{e}^{-\bar{\xi}\bar{\Omega} \pm \mathrm{j}\bar{\Omega}_D} \tag{12}$$

where $\mathrm{j} = \sqrt{-1}$, $a = 1 - \frac{1}{2}(1+\alpha)\Omega^2$, $b = \Omega\sqrt{1 - \frac{1}{4}(1+\alpha)^2\Omega^2}$ and $\bar{\Omega}_D$ and $\bar{\xi}$ are defined as follows:

$$\bar{\Omega}_D = \tan^{-1}\left(\frac{b}{a}\right) \tag{13}$$

$$\bar{\xi} = -\frac{\ln(a^2 + b^2)}{2\bar{\Omega}} \tag{14}$$

Another important quantity is the relative period error:

$$\frac{T - \bar{T}}{T} = 1 - \frac{\omega}{\bar{\omega}} \tag{15}$$

where $\bar{\omega}$ is the computed natural frequency and $\bar{T} = (2\pi)/\bar{\omega}$ and $T = (2\pi)/\omega$.

In order to have a bounded oscillatory response, the eigenvalues of the matrix $\mathbf{A}$ should be complex conjugates and $|\lambda_{1,2}| \leqslant 1$. These lead to

$$-1 \leqslant \alpha \leqslant \frac{2}{\Omega} - 1 \tag{16}$$

and

$$0 \leqslant \alpha \leqslant \frac{1}{\Omega^2} \tag{17}$$

Figure 1 plots the results of these two inequalities. If $\alpha = 0$, we can have maximum stability range $0 \leqslant \Omega \leqslant 2$. These two inequalities can be combined to obtain the following inequality for the range of $0 \leqslant \Omega \leqslant 2$:

$$0 \leqslant \alpha \leqslant \frac{2}{\Omega} - 1 \tag{18}$$

If α is appropriately chosen to meet the above conditions, favourable numerical dissipation can be achieved. From the currently available integration methods,[6,8–10,14,15] it can be found that the numerical damping $\bar{\xi}$ and the relative period error $(T - \bar{T})/T$ are functions of Ω, such as $F(\Omega)$ and $G(\Omega)$, respectively. In general, they are increasing functions with increasing positive slopes for an integration method having frequency-proportional damping. Thus, $\bar{\xi}$ and $\bar{\Omega}$ can be expressed as

$$\bar{\xi} = F(\Omega) \tag{19}$$

and

$$\bar{\Omega} = \frac{\Omega}{1 - G(\Omega)} \tag{20}$$

By substituting equations (19) and (20) into equation (14) where $(a^2 + b^2)$ is equal to A_2 as given in equation (9), we can obtain

$$\alpha = \left(\frac{1}{\Omega^2}\right)\{1 - e^{-[(2\Omega F(\Omega))/(1 - G(\Omega))]}\} \tag{21}$$

Obviously, the functions $F(\Omega)$ and $G(\Omega)$ must be carefully selected to satisfy equation (18).

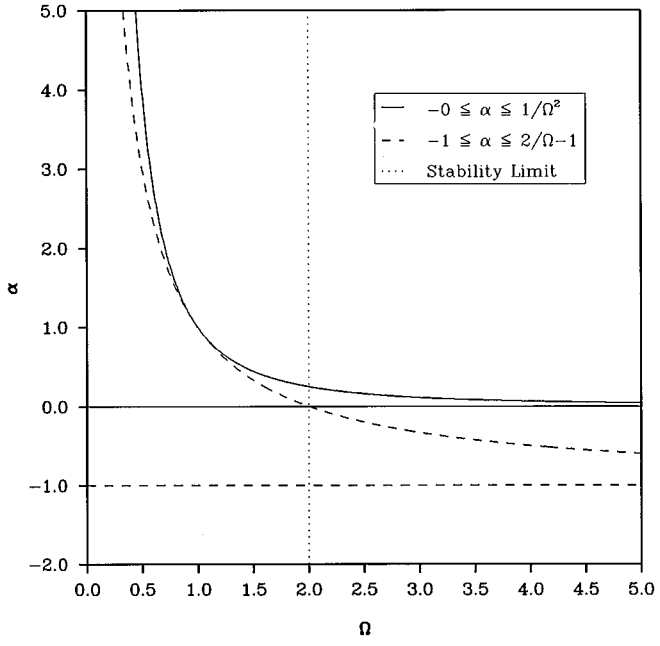

Figure 1. Boundaries of α-value

For simplicity, $F(\Omega)$ and $G(\Omega)$ are each assumed to be an increasing polynomial function of Ω with increasing positive slope and it may be assumed that:

$$F(\Omega) = p\Omega^q \tag{22}$$

$$G(\Omega) = r\Omega^s \tag{23}$$

where p, q, r, and s are appropriate positive constants. In addition, q and s must be greater than 1 in order to represent an increasing function with increasing positive slope. As a result, the $\bar{\Omega}$ and $\bar{\xi}$ of the algorithm can be obtained from equations (13) and (14) and have the following expressions:

$$\bar{\Omega} = \tan^{-1}\left[\frac{\Omega\sqrt{1 - \frac{1}{4}(1+\alpha)^2\Omega^2}}{1 - \frac{1}{2}(1+\alpha)\Omega^2}\right] \tag{24}$$

$$\bar{\xi} = -\frac{\ln(1 - \alpha\Omega^2)}{\bar{\Omega}} \tag{25}$$

We will expect that these two functions are different from the assumed functions as given in equations (19) and (20), since $F(\Omega)$ and $G(\Omega)$ are taken independently for the two mutually coupled functions.

The effects of p, q, r, and s are investigated through parametric studies and are shown in Figure 2. The parametric studies are conducted by considering $p = r = 0{\cdot}05$ and $q = s = 3$ as a basic case. This case is intentionally designed to possess the desired numerical damping, i.e., frequency-proportional damping. Other cases are performed by varying only one of the four constants. Figures 2(a)–2(d) show the variation of numerical damping with respect to p, q, r, and s, respectively.

Comparing Figures 2(a) and 2(b) with Figures 2(c) and 2(d), we can conclude that the variations of the constants p and q [i.e., $F(\Omega)$] have larger effects on numerical damping than those of r and s [i.e., $G(\Omega)$]. Figure 2(a) indicates that the curve moves upward with the increase of p value and all the curves can achieve the desired numerical dissipation. From the results of Figure 2(b), it shows that for $0 \leqslant \Omega \leqslant 1$, the curves move downward as q increases from 1 to 5 while for Ω between 1 and the stability limit, the curves move upward with the increase of p from 1 to 5. It seems that these cases with $q \geqslant 3$ can yield the desired numerical dissipation. Figures 2(c) and 2(d) indicate that the effects of r and s are not significant; especially at $0 \leqslant \Omega \leqslant 1$. It is likely that the numerical damping is independent of the function $G(\Omega)$ in this range.

Since the amount of the numerical damping is not significantly affected by the variation of the function $G(\Omega)$, it seems convenient to assume that $G(\Omega)$ is equal to zero. Thus, equation (21) reduces to

$$\alpha = \frac{1}{\Omega^2}(1 - \mathrm{e}^{-2p\Omega^{q+1}}) = \sum_{n=1}^{\infty}(-1)^{n+1}\left[\frac{(2p)^n}{n!}\right]\Omega^{n(2q+1)-2} \tag{26}$$

where Taylor's expansion has been applied in order to obtain a simple polynomial function when the series is truncated. If we choose $q = 3$, we have

$$\alpha = \sum_{n=1}^{\infty}(-1)^{n+1}p_n\Omega^{4n-2} = \sum_{n=1}^{\infty}(-1)^{n+1}p_n\left[\frac{k}{m}(\Delta t)^2\right]^{2n-1} \tag{27}$$

where $p_n = (2p)^n/n!$. The expression of α in terms of mass m, stiffness k and the size of time step Δt instead of Ω is beneficial, since for a large MDOF system, it avoids the need for solving an eigenvalue problem which is the most time consuming phase of the analysis for matrices of large order. Thus, q must be an odd number in order to yield the above expression of α.

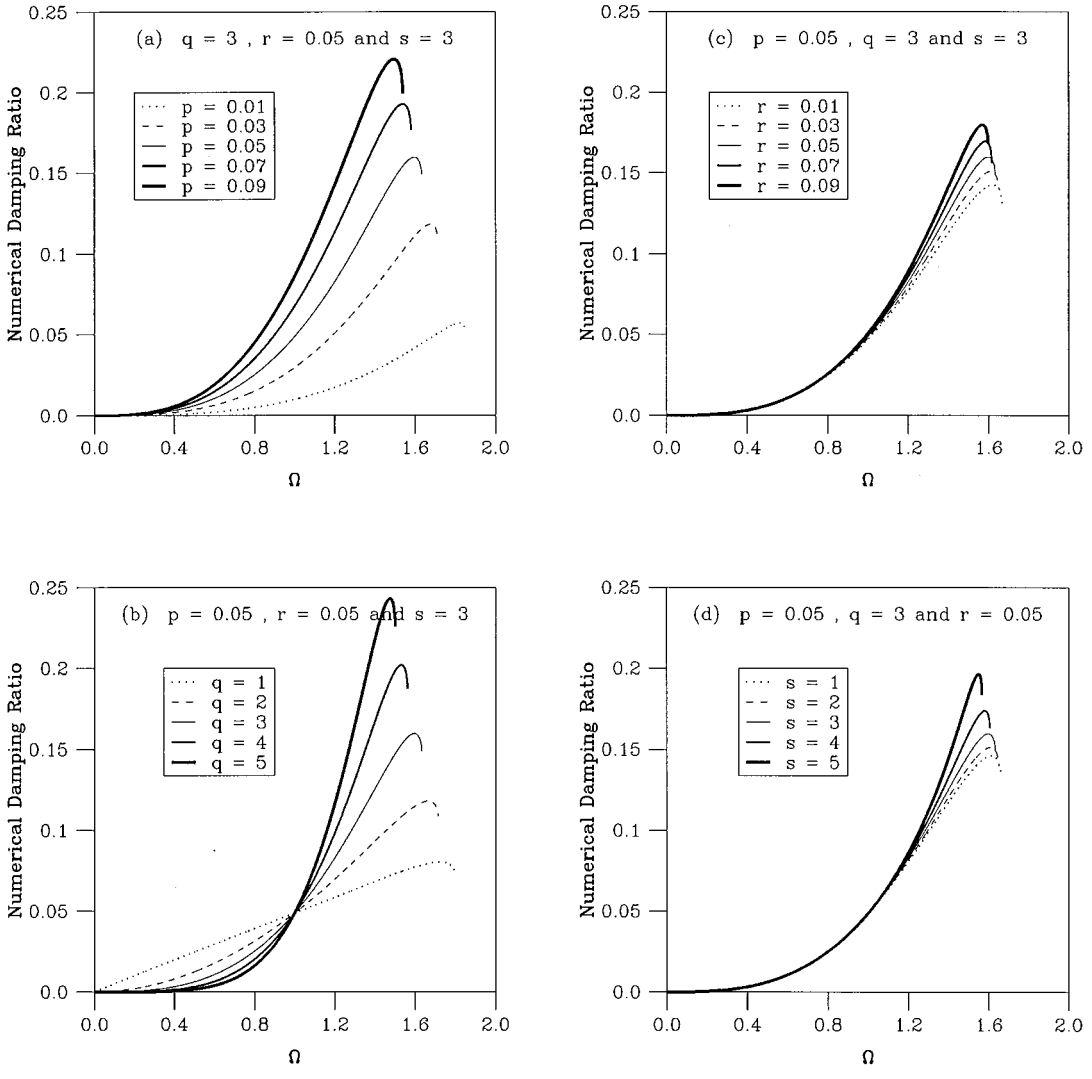

Figure 2. Parametric effects on variation of numerical damping vs. Ω

γ-function dissipative method

The other family of explicit methods can also be developed if $\alpha = \beta = 0$ is considered. Employing the same procedure for the derivation of α-function dissipative method, one has

$$\gamma = \frac{1}{2} + \sum_{n=1}^{\infty} (-1)^{n+1} p_n \Omega^{4n-2} = \frac{1}{2} + \sum_{n=1}^{\infty} (-1)^{n+1} p_n \left[\frac{k}{m} (\Delta t)^2 \right]^{2n-1} \tag{28}$$

By substituting α, β and γ for the α-function and γ-function dissipative methods into equation (5), we will obtain exactly the same eigenvalues for the two families of methods. This also can be seen by comparing equations (27) and (28) to yield $\alpha = \frac{1}{2} - \gamma$. Thus, the two families of methods possess exactly the same numerical characteristics.

COMPARISON OF ALGORITHMS

The following example is used to demonstrate the improved property of numerical dissipation for the α-function dissipative method by letting $\alpha = p_1(k/m)(\Delta t)^2$, $\beta = 0$, and $\gamma = \frac{1}{2}$, where only the first term of equation (40) is used. For the sake of comparison, the Newmark explicit method with γ-dissipation and the explicit predictor-corrector α-method[15] will also be investigated here. In order to have second-order accuracy for the explicit predictor–corrector α-method, the parameters are selected such that $-\frac{1}{3} \leqslant \alpha \leqslant 0$, $\beta = \frac{1}{4}(1 + \alpha)^2$ and $\gamma = \frac{1}{2} - \alpha$. Three different values of p_1, γ and α for the proposed schemes, for the Newmark explicit method with γ-dissipation, and for the explicit predictor–corrector α-method are used to illustrate the numerical characteristics of all three algorithms. These values for p_1 and γ were chosen to have about the same maximum numerical damping for each case while for the explicit predictor–corrector α-method, α values of $-0{\cdot}1$, $-0{\cdot}2$ and $-\frac{1}{3}$ were considered.

In Figure 3, the variations of numerical damping ratios with Ω are compared. The continuous control of the numerical dissipation in the proposed schemes is evident and this figure also shows that these algorithms possess the desired numerical dissipation. For the Newmark explicit method with γ-dissipation, the numerical damping is almost linearly proportional to Ω, which causes the lower modes to be damped too strongly. By contrast, for the proposed schemes, the damping curves have a zero slope at the origin and then turn upward gradually. This ensures less damping for lower modes and large enough numerical damping to damp out the spurious growth of higher modes. The explicit predictor–corrector α-method also shows the desired dissipative characteristics. For this method, the damping curve which yields the maximum numerical dissipation is the case of $\alpha = -\frac{1}{3}$. This curve almost coincides with the curve of the α-function dissipative method with $p_1 = 0.038$ if $\Omega \leqslant 1.4$. The damping curve with $p_1 = 0.038$ can move upward and leftward by increasing the value of p_1 for the α-function dissipative method while for the explicit predictor–corrector α-method, it is not able to shift the curve with $\alpha = -\frac{1}{3}$ either upward or leftward. It should be mentioned that

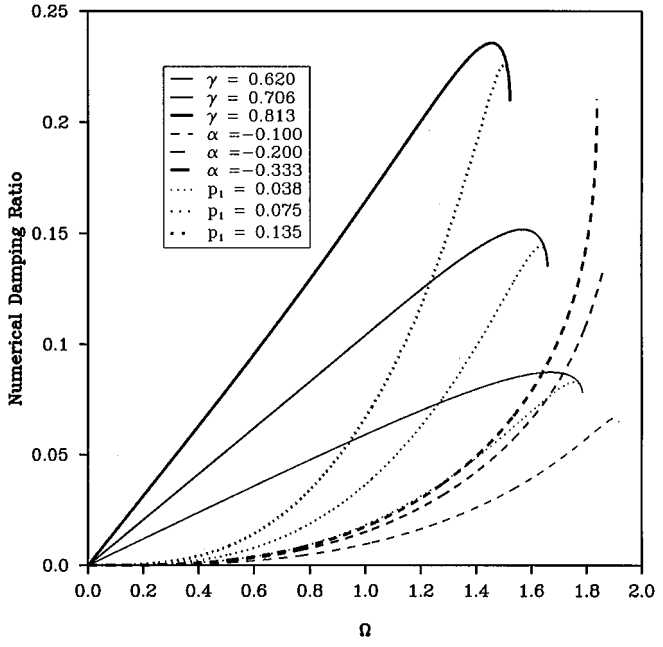

Figure 3. Variation of numerical damping ratio with Ω

the implementation for the predictor–corrector α-method is much more complex than for the proposed explicit methods since it generally requires an iterative procedure for a predictor–corrector method.

The local truncation error for each algorithm can be theoretically determined. From the expression of equation (7) and by substitution of α, β and γ for the proposed α-function dissipative method, we have

$$E = \tfrac{1}{12}\omega^2\Omega^2 u \tag{29}$$

The local truncation error for the Newmark explicit method with γ-dissipation is found to be

$$E = \left(\gamma - \frac{1}{2}\right)\omega\Omega\dot{u} \tag{30}$$

and that for the explicit predictor–corrector α-method is:

$$E = [\tfrac{1}{12} + \tfrac{1}{4}\alpha(1+\alpha)^2]\omega^2\Omega^2 u \tag{31}$$

Thus, both the proposed schemes and the explicit predictor–corrector α-method are of second-order accuracy while the Newmark explicit method with γ-dissipation is of only first-order accuracy if $\gamma > \frac{1}{2}$. This ensures the proposed schemes and the explicit predictor–corrector α-method possess better accuracy than that of Newmark explicit method with γ-dissipation. The local truncation error for the explicit predictor–corrector α-method is also less than the proposed schemes since the α value is chosen to be between $-\frac{1}{3}$ and 0. Figure 4 shows that the relative period error versus Ω for the various cases of each algorithm. These results confirm the indication of the local truncation error.

The spectral radii of various cases versus Ω has been plotted in Figure 5. The superiority of the dissipative properties of the proposed algorithms over the Newmark explicit method with γ-dissipation and the explicit predictor–corrector α-method is manifest from Figure 5. The abrupt turning point is the point at which complex conjugate eigenvalues bifurcate into two real, distinct eigenvalues.

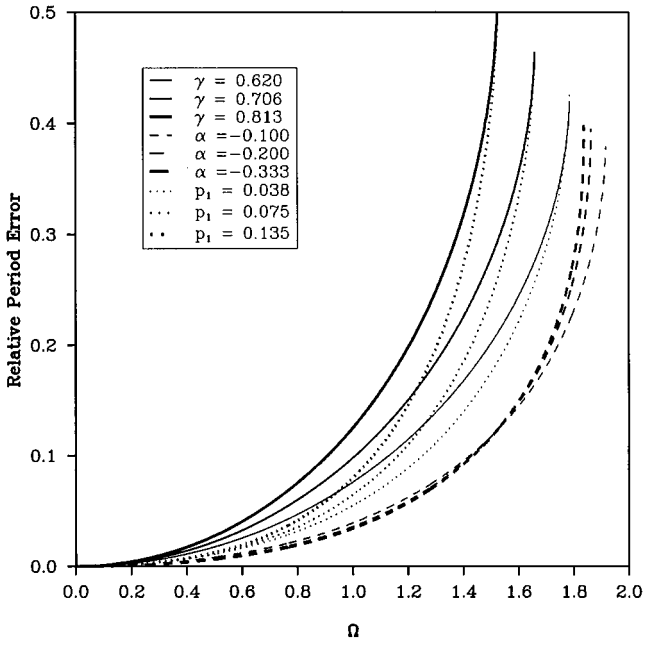

Figure 4. Variation of relative period error with Ω

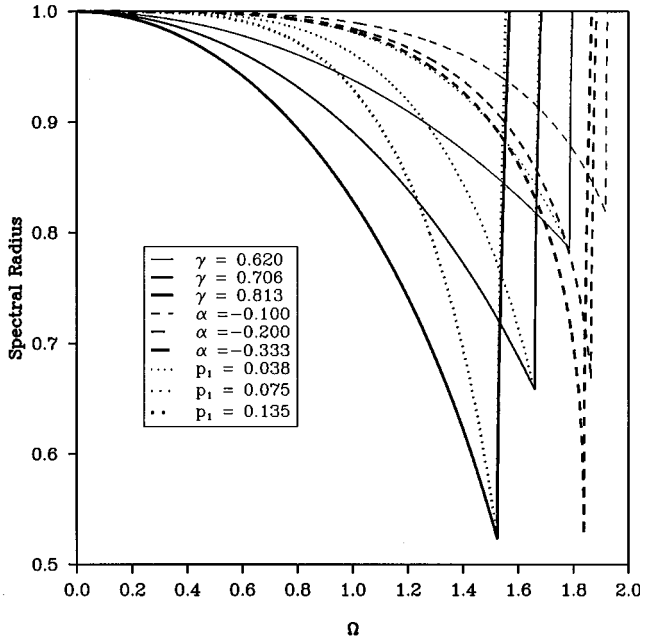

Figure 5. Variation of spectral radius with Ω

The higher-order terms of equation (27) or equation (28) can also be used to generate the favourable numerical damping. The equation $p_n = (2p)^n/n!$ need not be satisfied since $F(\Omega)$ can be arbitrary specified. Instead, they can be appropriately selected. If only the first two terms of equation (27) are considered, we have

$$\alpha = p_1\left(\frac{k}{m}\right)(\Delta t)^2 + p_2\left(\frac{k}{m}\right)^2(\Delta t)^4 \tag{32}$$

The results are shown in Figure 6 and they show that the numerical damping increases with the increase of the value of p_2 for a given Ω. Obviously, there are many other combinations that can be used to introduce the desired numerical damping for the proposed algorithms.

FORMULATION FOR MDOF SYSTEMS

The proposed schemes for a SDOF system can be generalized to a MDOF system, in which they have the following expressions:

$$\begin{gathered}\mathbf{M}\mathbf{a}_{i+1} + (\mathbf{I}+\boldsymbol{\alpha})\mathbf{K}\mathbf{d}_{i+1} - \boldsymbol{\alpha}\mathbf{K}\mathbf{d}_i = \mathbf{f}_{i+1} \\ \mathbf{d}_{i+1} = \mathbf{d}_i + (\Delta t)\mathbf{v}_i + (\Delta t)^2[(\tfrac{1}{2}\mathbf{I}-\boldsymbol{\beta})\mathbf{a}_i + \boldsymbol{\beta}\mathbf{a}_{i+1}] \\ \mathbf{v}_{i+1} = \mathbf{v}_i + (\Delta t)[(\mathbf{I}-\boldsymbol{\gamma})\mathbf{a}_i + \boldsymbol{\gamma}\mathbf{a}_{i+1}]\end{gathered} \tag{33}$$

where $\mathbf{I}$ is an identity matrix, $\mathbf{d}_i$, $\mathbf{v}_i$ and $\mathbf{a}_i$ are the vectors corresponding to the displacement, velocity, and acceleration at ith step, and $\boldsymbol{\alpha}$, $\boldsymbol{\beta}$ and $\boldsymbol{\gamma}$ are coefficient matrices. For α-function dissipative method, the coefficient matrices are

$$\boldsymbol{\alpha} = \sum_{n=1}^{\cdots} p_n[(\Delta t)^2\mathbf{K}\mathbf{M}^{-1}]^n, \qquad \boldsymbol{\beta} = 0, \qquad \boldsymbol{\gamma} = \tfrac{1}{2}\mathbf{I} \tag{34}$$

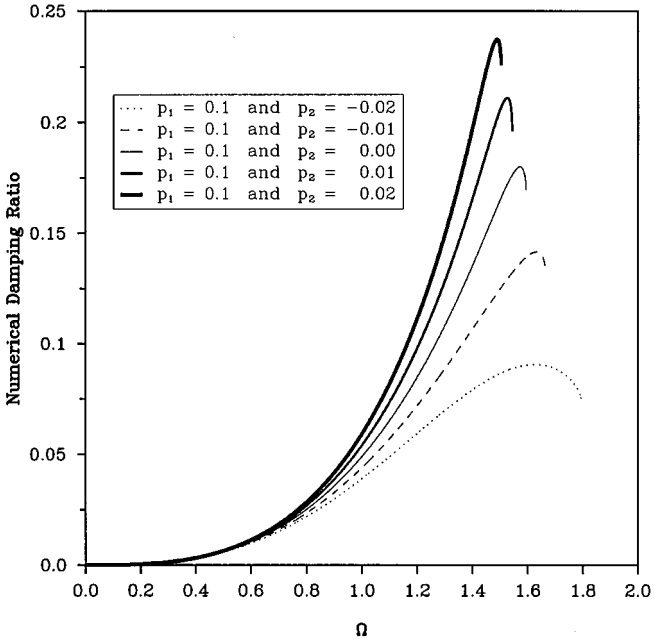

Figure 6. Numerical damping vs. Ω for proposed explicit methods

where p_n are appropriate constant coefficients. Although any combinations of all the terms can be used, the first one or two terms might be good enough to achieve the desired numerical damping. This method requires more computational effort than for the central difference method due to the extra computations of the product of global stiffness matrices. It is not cost-effective to extend the method beyond the p_1 term. These algorithms can be applied to pseudodynamic tests [10, 5] by transforming the governing equation as shown in equation (33) to

$$\mathbf{M}\mathbf{a}_{i+1} + (\mathbf{I} + \boldsymbol{\alpha})\mathbf{r}_{i+1} - \boldsymbol{\alpha}\mathbf{r}_i = \mathbf{f}_{i+1} \tag{35}$$

where $\mathbf{r}_i$ is the restoring force vector. It should be mentioned that the initial tangent stiffness is used in calculating the coefficient matrices which must be kept constant in each time step since the stiffness matrix is not known during a pseudodynamic test.

Obviously, the major difference between the α-dissipation method and the proposed algorithms is the coefficients. For α-dissipation method α, β and γ are scalar coefficients while for the proposed schemes $\boldsymbol{\alpha}$, $\boldsymbol{\beta}$ and $\boldsymbol{\gamma}$ are coefficient matrices which are functions of $\mathbf{M}^{-1}$, $\mathbf{K}$, and Δt

A NUMERICAL EXAMPLE

A 2-degree-of-freedom linear elastic shear beam type structure will be considered here. The unusual structure is intentionally chosen to have a high natural frequency in order to demonstrate the characteristic of the favourable numerical dissipation. The lumped masses for each story of the system are $m_1 = 1$ kg and $m_2 = 1$ kg and stiffness for each storey are $k_1 = 15000$ N/m and $k_2 = 100$ N/m. The natural frequencies of the structure are 9·97 rad/s and 122·88 rad/s and their corresponding mode shapes are

$$\Phi = \begin{bmatrix} 0{\cdot}00667 & 0{\cdot}99998 \\ 0{\cdot}99998 & -0{\cdot}00667 \end{bmatrix} \tag{36}$$

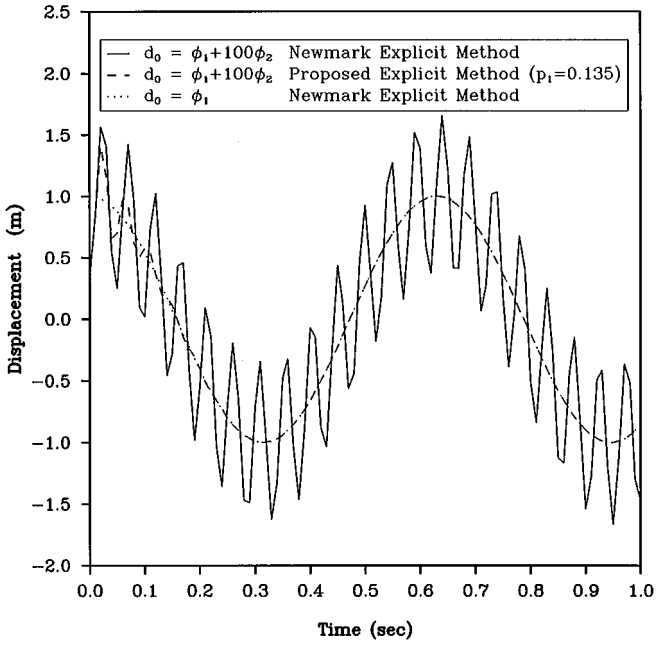

Figure 7. Free vibration response of the second storey

where each column corresponds to each mode shape. The mode shapes are scaled so that $\|\phi\| = \sqrt{(\phi^{\mathrm{T}}\phi)} = 1$.

Figure 7 demonstrates that the α-function dissipative method can effectively damp out the second mode. The dotted line represents the free vibration responses of the structure with $\mathbf{d}_0 = (0{\cdot}00667, 0{\cdot}99998)^{\mathrm{T}}$ which is composed of the first mode only. The other two lines are the solutions of the system subjected to the initial displacement $\mathbf{d}_0 = (100{\cdot}00467, 0{\cdot}33298)^{\mathrm{T}}$, which adds one hundred times of the second mode shape to the previous $\mathbf{d}_0$ [see equation (36)]. The dotted and solid lines are obtained by using the Newmark explicit method while the dashed line is obtained by using the α-function dissipative method with the first term only, as shown in equation (34). The coefficient p_1 is taken to be 0·135 and the properties of this algorithm were shown in Figures 3–5. The time step used in all the computations is 0·01 s. Obviously, the proposed method can filter out the second mode very quickly and hardly affects the first mode at all, since after about 0·2 second the dotted and dashed lines coincide. Actually, this result can be completely explained by the Figure (3) since the values of $\omega(\Delta t)$ for each mode are about 0·01 and 1·22 which correspond to about zero and 12 per cent numerical damping. Thus, the first mode is almost not affected and the second mode can be damped out very quickly.

CONCLUSIONS

Two new families of conditionally stable, one-step algorithms for structural dynamics have been developed and are shown to possess significantly improved numerical damping which can be continuously controlled. In particular, the methods are of second-order accuracy and it is possible to achieve zero damping. It was shown that the new families of methods possess better accuracy than the Newmark explicit method with γ-dissipation since all the proposed algorithms are second-order methods while the Newmark explicit method with γ-dissipation is a first-order method.

These algorithms are very useful for pseudodynamic test methods since the spurious growth of higher-mode response can be eliminated by the numerical damping while lower modes are obtained accurately.

ACKNOWLEDGEMENTS

The author is grateful to acknowledge that this study is financially supported by the National Science Council, Taiwan, R.O.C., under Grant No. NSC-86-2211-E-319-001.

REFERENCES

1. S. Y. Chang and S. A. Mahin, 'Two new implicit algorithms of pseudodynamic test methods', *M. Eng. Thesis*, University of California, Berkeley, 1992.
2. M. Nakashima, T. Kaminosomo and M. Ishida, 'Integration techniques for substructure pseudodynamic test', *Proc. 4th U.S. nat. conf. on earthquake eng.,* Vol. 2, 1990, pp. 515–524.
3. P. B. Shing, M. T. Vannan and E. Carter, 'Implicit time integration for pseudodynamic tests', *Earthquake Engng. Struct. Dyn.* **20**, 551–576 (1991).
4. C. R. Thewalt and S. A. Mahin, 'An unconditionally stable hybrid pseudodynamic algorithm', *Earthquake Engng. Struct. Dyn.* **24**, 723–731 (1995).
5. P. B. Shing and S. A. Mahin, 'Elimination of spurious higher-mode response in pseudodynamic test', *Earthquake Engng. Struct. Dyn.* **15**, 425–445 (1987).
6. K. J. Bathe and E. L. Wilson, 'Stability and accuracy analysis of direct integration methods, *Earthquake Engng. Struct. Dyn.* **1**, 283–291 (1973).
7. J. C. Houbolt, 'A recurrence matrix solution for the dynamic response of elastic aircraft', *J. aeronaut. sci.* **17**, 540–550 (1950).
8. H. M. Hilber, 'Analysis and design of numerical integration methods in structural dynamics', *EERC Report No. 76-29*, Earthquake Engineering Research Center, University of California, Berkeley, CA, November 1976.
9. H. M. Hilber, T. J. R. Hughes and R. L. Taylor, 'Improved numerical dissipation for time integration algorithms in structural dynamics', *Earthquake Engng. Struct. Dyn.* **5**, 283–292 (1977).
10. P. B. Shing and S. A. Mahin, 'Cumulative experimental errors in pseudodynamic tests', *Earthquake Engng. Struct. Dyn.* **15**, 409–424 (1987).
11. R. W. Clough and J. Penzien, '*Dynamics of Structures*,' McGraw-Hill, New York, 1967.
12. N. M. Newmark, 'A method of computation for stuctural dynamics', *J. eng. mech. div. ASCE* **85**, 67–94 (1959).
13. T. Belytschko and T. J. R. Hughes, *Computational methods for transient analysis*, Elsevier, North-Holland, 1983.
14. H. M. Hilber and T. J. R. Hughes, 'Collocation, dissipation, and 'overshoot' for time integration schemes in structural dynamics', *Earthquake Engng. Struct. Dyn.* **6**, 99–118 (1978).
15. I. Miranda, R. M. Ferencz and T. J. R. Hughes, 'An improved implicit–explicit time integration method for structural dynamics', *Earthquake Engng. Struct. Dyn.* **18**, 643–653 (1989).

